Synchronizing Bloch-Oscillating Free Carriers in Moiré Flat Bands

Ali Fahimniya,[1] Zhiyu Dong,[1] Egor I. Kiselev,[2] and Leonid Levitov[1]
[1]Physics Department, Massachusetts Institute of Technology, Cambridge, Massachusetts 02139, USA
[2]Institut fur Theorie der Kondensierten Materie, Karlsruher Institut fur Technologie, 76131 Karlsruhe, Germany

(Received 25 November 2020; accepted 18 May 2021; published 25 June 2021)

Achieving Bloch oscillations of free carriers under a direct current, a long-sought-after collective many-body behavior, has been challenging due to stringent constraints on the band properties. We argue that the flat bands in moiré graphene fulfill the basic requirements for observing Bloch oscillations, offering an appealing alternative to the stacked quantum wells used in previous work aiming to access this regime. Bloch-oscillating moiré superlattices emit a comblike spectrum of incommensurate frequencies, a property of interest for converting direct currents into high-frequency currents and developing broadband amplifiers in terahertz domain. The oscillations can be synchronized through coupling to an oscillator mode in a photonic or plasmonic resonator. Phase-coherent collective oscillations in the resonant regime provide a realization of current-pumped terahertz lasing.

DOI: 10.1103/PhysRevLett.126.256803

Bloch oscillations, arising when electrons are driven through a perfect crystal lattice by an electric field, are an iconic example of a coherent dynamics in quantum many-body systems [1,2]. The oscillations are at the same frequency for all carriers, for a one-dimensional lattice given by $\omega = eEa/\hbar$ with E the field strength and a the lattice period. Besides the obvious fundamental appeal, this behavior has long been eyed as a promising way to convert direct currents into high-frequency currents [3]. Wide interest in this phenomenon stems from the expectation that it may help fill the infamous "terahertz gap," leading to radiation emitters and detectors operating in this frequency range [4–6].

While Bloch oscillations have long been immortalized in textbooks, realizing them in solids has proven to be a challenging task. Achieving this regime requires overcoming several obstacles. One is the dephasing due to electron energy loss to phonons. To suppress phonon emission exceptionally narrow electronic bands of width smaller than the optical phonon energy must be used. Another is the dephasing due to disorder scattering. Experimental efforts so far mainly focused on narrow minibands in synthetic MBE-grown semiconductor superlattices [6–9]. These systems cleared a number of key milestones on the road toward achieving Bloch oscillations. They display the signatures indicative of Bloch oscillations such as negative differential conductivity $dI/dV < 0$, recurrence and ringing in the optical pump-probe measurements, Wannier-Stark (WS) ladders and, last but not least, optical gain [6–9]. However, upon the injection current approaching the relevant parameter range the superlattice systems develop instabilities and show a complex noisy behavior due to the onset of switching and formation of electric domains. This behavior presents the main obstacle to achieving the collective globally synchronized Bloch oscillations [10–12].

Meanwhile, recently Bloch oscillations were achieved in cold atom systems, using Bloch minibands in optical lattices [13–17]. This proof-of-principle demonstration has greatly improved our understanding of the underlying physics [18,19] and strengthened interest in demonstrating electronic Bloch oscillations.

Given the difficulties encountered in semiconducting superlattices it is natural to seek other systems that meet the requirements for achieving Bloch oscillations. One enticing opportunity is offered by the recently introduced moiré superlattices in twisted bilayer graphene, a material that hosts electron bands that are tunable by the twist angle [20–25]. For twist angles $\theta \lesssim 2°$ the moire electron bands are considerably narrower than the optical phonon energy (∼200 meV), becoming as narrow as $J \lesssim$ 10–20 meV near "magic" values of the twist angle $\theta \sim 1°$. Such bandwidths are sufficient to eliminate the optical phonon emission, the main obstacle to observing coherent Bloch oscillations in widebands.

The moiré graphene also clears other key requirements for observing Bloch oscillations. One is weak disorder scattering. Since the narrow bands are formed in a solid with a pristine near-perfect atomic order, they are less susceptible to disorder than the bands in synthetic MBE-grown semiconductor superlattices. This is manifested in a high carrier mobility and ballistic carrier transport observed over micron length scales at $T = 0$ [24,25]. Estimating the scattering time as $\tau = l/v_F$ with the mean free path $l \sim 1$ μm and velocity v_F of about $1/30$ of the graphene monolayer value 10^6 m/s gives $\tau \sim 3 \times 10^{-11}$ s, a value comparable to that of graphene monolayer. The scattering rate can therefore be as low as $\gamma_{\rm dis} \sim 10^{-2} J$. The two-

dimensional character of moiré graphene will also help to suppress the instability toward the formation of electric field domains that hindered experiments in the stacks of quantum wells [6]. In the moiré setup the electric current can be driven in the graphene plane in a manner that maintains the translation invariance of the system and does not cause local charging. Indeed, gating is known to maintain a spatially uniform carrier density even under moderate to high currents.

Other appealing properties of moiré graphene are the lack of Zener transitions, suppressed by sizable minigaps, and the weakness of the coupling between electrons and long-wavelength acoustic phonons [26–28]. Further, the relatively large periodicity of moiré superlattices ($a \sim 10$ nm) reduces the required E field values:

$$\gamma = \max[\gamma_{\rm ph}, \gamma_{\rm dis}] < \omega_B < J/\hbar, \qquad \omega_B = eEa/\hbar. \tag{1}$$

Using moderate E fields will help to avoid the WS localization effects and charge instabilities.

A key assumption is that phonon emission can remain relatively weak despite rate enhancement due to the high density of states in moiré bands and an out-of-equilibrium carrier state created under an applied current. These expectations are supported by a detailed analysis of phonon emission [29], predicting emission rates which drop upon an increase in the flat-band width and a growing E field. Detuning away from the magic twist angle reduces the density of states that governs phonon emission. Likewise, an E field tunes the WS states out of resonance, abruptly quenching phonon emission.

Importantly, although all free carriers Bloch oscillate with identical frequencies, these oscillations are *asynchronous,* as the oscillation phases are totally random and uncorrelated for different carriers. Therefore, in order to achieve collective continuous-wave Bloch oscillations driven by a direct current, movements of different carriers must be synchronized. We outline a way to achieve this through coupling of the current-carrying channel to an oscillator mode in a terahertz resonator. The resonator frequency depends on system parameters, whereas the Bloch frequency is tunable by varying the applied electric field. As illustrated in Fig. 1, this system develops an instability toward collective oscillations at a Bloch frequency when the latter is close to the oscillator frequency. In practice, the oscillator can be realized as a terahertz photonic or plasmonic resonator in a 2D or a 3D architecture [6,30–34]. An alternative route to achieve synchronization is through coupling to an intrinsic collective mode, excitonic or plasmonic. Phase-coherent oscillations achieved in this regime represent a realization of electrically pumped terahertz lasing.

Before considering the synchronization problem we summarize the basic picture of the free-carrier Bloch oscillations in superlattices. In superlattices of dimension

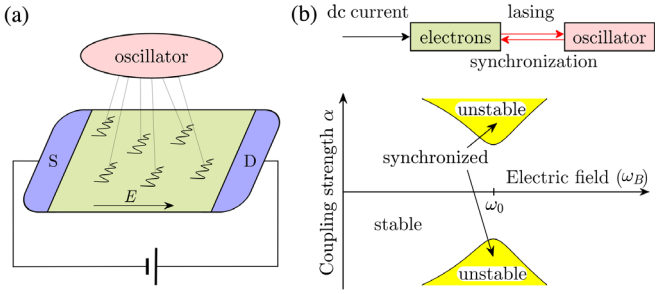

FIG. 1. (a) Bloch-oscillating electrons synchronized by coupling to an oscillator mode. A dc electric field $\boldsymbol{E}$ drives free-carrier oscillations with frequency ω_B (wavy lines). The oscillations are at the same frequency for all carriers but are asynchronous (not in phase). Synchronized oscillations are achieved through coupling to an oscillator mode, depicted by the thin lines. (b) A phase diagram showing the stable and unstable regimes in which Bloch oscillations are asynchronous and synchronized, respectively. The carrier scattering rate γ is taken to be equal to the oscillator damping γ_0 [see Eq. (11)]; phase diagrams for unequal γ and γ_0 are discussed in [29]. The Bloch frequency ω_B on the x axis is proportional to the electric field; ω_0 is the oscillator frequency, the coupling strength α between electrons and the oscillator is defined in Eq. (9). Instability is easiest to achieve when ω_B is tuned close to ω_0. The flowchart on the top shows the relationship between different degrees of freedom: the dc current drives free-carrier oscillations; these, synchronized by the oscillator, pump energy into the it (the lasing effect).

$D \geq 2$ different carriers can move at different angles relative to the applied field [18,19,35–37]. Nevertheless, the main properties of the one-dimensional Bloch oscillations persist. The Bloch frequencies remain discrete, taking values identical for all carriers in the system. A new aspect is that different harmonics of the band dispersion produce oscillations with several different discrete frequencies. These frequencies are in general incommensurate with one another, forming a comblike spectrum pictured in Figs. 2 and 3.

The frequency comb dependence on the electric field orientation is described by the geometric construction illustrated in Fig. 2. Namely, possible frequencies are given by the projections of different Bravais lattice vectors $\boldsymbol{a}_l = n_1\boldsymbol{a}_1^{(0)} + n_2\boldsymbol{a}_2^{(0)}$ on the applied field $\boldsymbol{E}$:

$$\omega_l = \frac{e}{\hbar}\boldsymbol{E}\cdot\boldsymbol{a}_l = \frac{e}{\hbar}Ea_l\cos(\theta-\theta_l). \tag{2}$$

The dependence of the frequencies ω_l on the orientation and strength of the field $\boldsymbol{E}$, as well as the tunability of moiré superlattices by the twist angle, provide knobs that will facilitate achieving Bloch oscillations in moiré graphene.

This result can be illustrated by considering a general tight binding band on a monoatomic lattice,

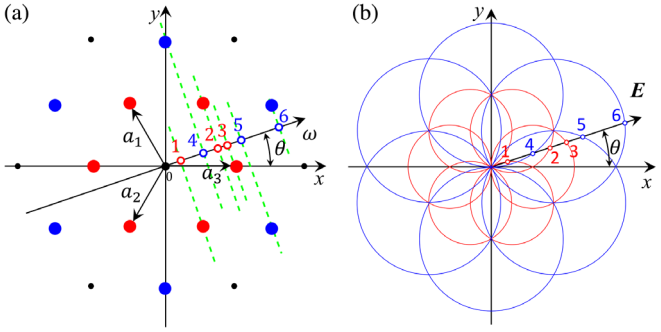

FIG. 2. (a) Geometric construction of the frequency comb for Bloch oscillations, Eq. (2), at a generic electric field orientation. Frequencies ω_l are found by projecting the real-space Bravais lattice points (solid circles) onto the 1D line parallel to $\boldsymbol{E}$ (black arrow) as indicated by dashed green lines. The shortest and next-shortest vectors are shown as red and blue dots. Hollow circles, found by projection, give the frequencies in Eq. (2), where the emitted noise power $P(\omega)$ peaks. (b) Visualization of the comb ω_l angle dependence vs $\boldsymbol{E}$ orientation relative to the superlattice.

$$\epsilon(\boldsymbol{k}) = \sum_{l=1,2...} -2J_l \cos(\boldsymbol{k}\cdot\boldsymbol{a}_l). \tag{3}$$

The Bravais lattice vectors $\boldsymbol{a}_l$ describe hopping between different pairs of lattice sites, either nearest-neighbor or non-nearest-neighbor. Bloch-oscillating free carriers obey quasiclassical equations of motion

$$\hbar\frac{d\boldsymbol{k}}{dt} = e\boldsymbol{E}, \tag{4}$$

generating a linear time dependence $\boldsymbol{k}(t) = (e/\hbar)\boldsymbol{E}t + k_0$ with the linear part identical for all carriers and a carrier-specific initial value k_0. With this band structure and an electric field of a generic orientation, $\boldsymbol{E} = E(\cos\theta, \sin\theta)$,

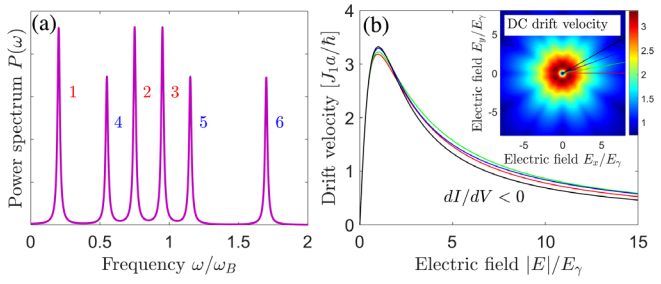

FIG. 3. (a) The comblike frequency spectrum of current fluctuations, Eq. (5), consisting of finite-width resonances at the discrete frequency values ω_l, Eq. (2). Frequency units are $\omega_B = (e/\hbar)Ea$, the power spectrum $P(\omega)$ is in arbitrary units. The field orientation and labeling of different peaks match those in Fig. 2. (b) The direct-current drift velocity, Eq. (6). Shown is the full dependence (inset) and traces for several different field orientations. Bloch oscillations occur for field strength $E > E_\gamma = \hbar\gamma/ea$; negative differential conductivity $dI/dV < 0$ is a hallmark of this regime.

the frequencies at which the time-dependent velocity of the electrons $\boldsymbol{v}(t) = (1/\hbar)\nabla_k\epsilon(\boldsymbol{k})|_{\boldsymbol{k}=(e/\hbar)\boldsymbol{E}t+k_0}$ will oscillate are given by $\boldsymbol{a}_l$ projected on $\boldsymbol{E}$, Eq. (2). The resulting dependence of the frequencies ω_l on the orientation of $\boldsymbol{E}$ is described by families of circles pictured in Fig. 2.

Physically, discrete frequency values arise because electron trajectories sweep the (reduced) Brillouin zone (BZ) of a two-dimensional crystal in the direction set by the $\boldsymbol{E}$ vector. Every time an electron reaches a zone boundary it umklapps to the opposite side and continues forward, winding around the BZ at different frequencies in different crystal axes directions. In that, the time-averaged rate of winding around BZ along the direction of $\boldsymbol{E}$ is the same for all carriers. This leads, for a general field orientation, to a quasiperiodic dynamics characterized by two fundamental frequencies which depend only on the field $\boldsymbol{E}$ and lattice periodicity as described in Eq. (2), wherein $\omega_l = n_1\omega_1 + n_2\omega_2$ in agreement with the geometric construction in Fig. 2.

In the presence of momentum-relaxing scattering the frequency spectrum broadens into a sum of finite-width resonances centered at $\omega = \omega_l$. The quantity of interest is the autocorrelation function of current fluctuations $P(\omega) = \frac{1}{2}\int_{-\infty}^{\infty}\langle\delta\boldsymbol{j}(t)\cdot\delta\boldsymbol{j}(t+\tau)\rangle e^{-i\omega\tau}d\tau$ which describes the spectrum of electric noise emitted by the system. Simple analysis predicts a comblike emitted power spectrum

$$P(\omega) = \sum_l \frac{P_l}{(\omega-\omega_l)^2+\gamma^2} \tag{5}$$

(see [29]). The Bloch oscillation regime corresponds to nonoverlapping resonances. Since the frequencies ω_l are proportional to the applied field $\boldsymbol{E}$ the oscillations appear when the field strength exceeds a threshold set by momentum-relaxing scattering, $E_\gamma = \gamma\hbar/ea$. At lower fields the resonances merge into a broadband noise spectrum, indicating a suppression of the oscillations.

In the Bloch oscillation regime the dc drift velocity exhibits negative differential conductivity $dI/dV < 0$, a characteristic behavior that provides a clear signature of this regime. A direct calculation [29] predicts

$$\boldsymbol{v}_{\rm dc} = \sum_l \boldsymbol{a}_l \frac{2J_l f_l}{\hbar}\frac{\gamma\omega_l}{\gamma^2+\omega_l^2}, \qquad f_l = \sum_k f_0(k)e^{i\boldsymbol{a}_l\boldsymbol{k}}, \tag{6}$$

with $f_0(k)$ the steady-state momentum distribution. The dependence on the field E is linear at small $E < E_\gamma$ and falls off as $1/E$ at large $E > E_\gamma$. Interestingly, current depends on the dimensionless quantity E/E_γ in a way that is independent of the specific value of γ. This behavior is illustrated in Fig. 3(b). The drift velocity for electric fields in different directions is shown in the inset.

Next, we turn to the discussion of Bloch oscillations synchronized by coupling to an external oscillator mode:

$$H = \sum_i [\epsilon(\boldsymbol{p}_i) - e\boldsymbol{E}\boldsymbol{x}_i - \alpha Q x_i] + \frac{1}{2m}P^2 + \frac{\omega_0^2 m}{2}Q^2. \quad (7)$$

Here, $\epsilon(\boldsymbol{p})$ is the band dispersion, $\boldsymbol{p}_i$ and $\boldsymbol{x}_i$ are the momenta and coordinates of the electrons; P and Q are the momentum and amplitude of the oscillator. The Bloch electron coupling to the oscillator and the external field is through potentials $U(\boldsymbol{x}_i) = -e\boldsymbol{E}\boldsymbol{x}_i - \alpha Q x_i$ seen by each of the electrons. In this approach we ignore the direct carrier-carrier interactions, treating electron dynamics in a free-particle approximation. Bloch oscillations are driven by the electric field E, the term $-\alpha Q x_i$ describes coupling of the electrons to the oscillator mode. In practice the oscillator can be realized as, e.g., a terahertz photonic or plasmonic resonator [6,30–34].

Starting from the equations of motion originating from the Hamiltonian above, we wish to integrate out the carrier degrees of freedom and derive a closed-form dynamics for the oscillator. For that purpose we solve the equations of motion for the ith electron beginning from the time $t_i' < t$ when its state was last reset by scattering and the Hamiltonian dynamics described by Eq. (7) had started.

The full set of equations of motion for the electrons and the oscillator is

$$\dot{\boldsymbol{p}}_i = -\frac{\partial H}{\partial \boldsymbol{x}_i} = e\boldsymbol{E} + \alpha Q(t), \qquad \dot{\boldsymbol{x}}_i = \frac{\partial H}{\partial \boldsymbol{p}_i} = \frac{\partial \epsilon(\boldsymbol{p}_i)}{\partial \boldsymbol{p}_i},$$
$$\dot{P} = -m\omega_0^2 Q + \sum_i \alpha x_i, \qquad \dot{Q} = P/m. \quad (8)$$

Eliminating $P(t)$ yields a second-order equation of motion for the oscillator mode $Q(t)$, driven by an external force given by a sum of contributions due to the electrons

$$\ddot{Q}(t) + \omega_0^2 Q(t) = f(t), \qquad f(t) = \frac{\alpha}{m}\sum_i x_i(t). \quad (9)$$

Importantly, the cumulative effect due to the electrons, given by the quantity $f(t)$, gives rise to a "memory effect" in the oscillator dynamics. Each term in the sum $\sum_i x_i(t)$ is given by a solution of the equations of motion for $x_i(t)$ and $p_i(t)$, Eq. (8), initialized at an earlier random time $t_i' < t$. The oscillator dynamics $Q(t)$, $P(t)$ during the time intervals $t_i' < \tau < t$ affects the electron states $x_i(t)$, $p_i(t)$, giving rise to a backaction $f(t) = (\alpha/m)\sum_i x_i(t)$ with the dynamical memory originating from the dependence on $Q(\tau)$ and $P(\tau)$ at the earlier times $\tau < t$.

The feedback due to this memory effect enables synchronization of Bloch dynamics, resulting in a macroscopic oscillating current generated by Bloch-oscillating electrons. To describe the instability we compute the backaction term linearized in $Q(t')$ (the analysis is lengthy but straightforward, see [29]). Substituting the result in Eq. (9) gives a characteristic equation for ω of the form

$$\omega_0^2 - \omega^2 = \frac{i\lambda}{\omega}\left(\frac{\gamma^2}{(\gamma^2+\omega_B^2)(\gamma - i\omega)} + \frac{\gamma}{(\omega + i\gamma)^2 - \omega_B^2}\right), \quad (10)$$

where we defined $\lambda = N(\alpha^2 a v_0/m\hbar)$ with N the total number of Bloch-oscillating electrons.

The system becomes unstable when Eq. (10) admits solutions in the upper half-plane of complex ω. Before exploring this instability we inspect, as a sanity check, the regime of highly damped Bloch oscillations $\gamma \gg \omega_B, \omega_0$. In this case, Eq. (10) reads $\omega_0^2 - \omega^2 = (i\lambda/\omega\gamma)$. At large γ, the roots of this equation are close to $\pm\omega_0$. Writing $\omega = \pm\omega_0 + \Delta\omega$, at leading order in $1/\gamma$ we find $\Delta\omega = -(i\lambda/2\omega_0^2\gamma)$. The negative imaginary part indicates that no instability arises in this regime, i.e., the driven system is stabilized by high damping.

A very different situation occurs at weak damping $\gamma \ll \omega_B, \omega_0$. The new behavior is simplest to understand close to the resonance between the oscillator and Bloch frequencies, $\omega_0 \approx \omega_B$. For ω values near the resonance, where the last term in Eq. (10) dominates, we can ignore the first nonresonant term. This gives

$$[\omega_0^2 - (\omega + i\gamma_0)^2][(\omega + i\gamma)^2 - \omega_B^2] = \frac{i\lambda\gamma}{\omega}. \quad (11)$$

Here, we added the oscillator damping rate γ_0. Working near the resonance and expanding in a small $\delta\omega = \omega - \omega_0 \ll \omega_0 \approx \omega_B$ to obtain the complex frequency roots positioned near ω_0, the characteristic equation becomes

$$(\omega - \omega_0 + i\gamma_0)(\omega + i\gamma - \omega_B) = -i\eta/4, \qquad \eta = \frac{\lambda\gamma}{\omega_0^3}. \quad (12)$$

The properties of Eq. (12) are particularly straightforward when $\gamma_0 = \gamma$. In this case, the roots are

$$\omega_{1,2} = -i\gamma + \frac{\omega_B + \omega_0 \pm \sqrt{(\omega_B - \omega_0)^2 - i\eta}}{2}. \quad (13)$$

The system is stable if $\mathrm{Im}\omega_{1,2} < 0$ and unstable otherwise. Using the identity

$$\mathrm{Im}(\sqrt{x - i\eta}) = -\mathrm{sgn}\eta\sqrt{\frac{\sqrt{x^2+\eta^2} - x}{2}} \quad (14)$$

with $x = (\omega_B - \omega_0)^2$, the condition for the instability becomes

$$\eta^2 > [(\omega_B - \omega_0)^2 + 4\gamma^2]16\gamma^2. \quad (15)$$

This criterion predicts the Bloch frequency ω_B and the coupling strength λ values for which an instability toward a

synchronized dynamics may occur, giving the phase diagram shown in Fig. 1. As expected on general grounds, the instability is easiest to achieve when Bloch oscillations are in resonance with the oscillator, $\omega_B = \omega_0$. Tuning away from the resonance suppresses the instability. The instability signals the onset of a collective regime in which Bloch-oscillating electrons become synchronized through coupling to the oscillator mode.

A wider variety of collective regimes can be achieved by varying the oscillator damping γ_0. High and low damping values, $\gamma_0 \gg \gamma$ and $\gamma_0 \ll \gamma$, favor synchronization and lasing, respectively. In both cases the instability toward collective dynamics can occur not only on the resonance $\omega_B \approx \omega_0$ but also away from it in a relatively wide range of E fields, $\omega_B < \omega_0$ for synchronization and $\omega_B > \omega_0$ for lasing (see [29]). We note that the lasing regime can also be understood in terms of a negative ac conductivity that enables gain of terahertz radiation [5,10–12].

An intriguing question for future work is the role of electron interactions. Several interesting regimes can be envisioned depending on the relation between carrier concentration and the localization radius of WS states $r_0 \sim J/eE$. At high carrier concentration, $nr_0^2 \gg 1$, the interactions will act to dephase the oscillations, producing an asynchronous Bloch-oscillating electron gas. To the contrary, at low carrier concentration $nr_0^2 \ll 1$, the interactions will tend to create a spatially ordered Wigner solid of localized Bloch-oscillating carriers. Ordering will stabilize oscillations and facilitate synchronization.

Another question of interest is the effect of thermal fluctuations and noise. While the electron temperature under a strong direct current is expected to be high, in the architecture considered above the temperature of an external oscillator is naturally decoupled from that of electrons. The oscillator will remain cold and provide a synchronizing feedback on the electron subsystem.

In summary, the unique electronic properties of the flat bands in moiré graphene, such as the bandwidth considerably narrower than the optical phonon energy, the ~10 nm-large superlattice periodicity and relatively high mobility, will facilitate observing the Bloch oscillations. The two-dimensional nature of the system offers additional benefits: the carriers, which are fully exposed, can be coupled to a nearby oscillator mode that will synchronize their movements to enable phase-coherent collective oscillations, a regime in which current-pumped synchronization and terahertz lasing can be realized and explored.

This work was supported by the Science and Technology Center for Integrated Quantum Materials, NSF Grant No. DMR-1231319; and Army Research Office Grant No. W911NF-18-1-0116 (L. L.). E. K. acknowledges financial support by the Research Travel Grant of the Karlsruhe House of Young Scientists (KHYS).

[1] N. W. Ashcroft and N. D. Mermin, *Solid State Physics* (Saunders, Philadelphia, 1976).
[2] A. B. Pippard, *The Dynamics of Conduction Electrons* (Gordon and Breach Science Publishers, Inc., New York, 1965).
[3] L. Esaki and R. Tsu, Superlattice and negative differential conductivity in semiconductors, IBM J. Res. Dev. **14**, 61 (1970).
[4] S. A. Ktitorov, G. S. Simin, and V. Y. Sindalovskii, Bragg reflections and the high-frequency conductivity of an electronic solid-state plasma, Fiz. Tverd. Tela **13**, 2230 (1971) [Sov. Phys. Solid State **13**, 1872 (1972)].
[5] H. Kroemer, On the nature of the negative-conductivity resonance in a superlattice Bloch oscillator, arXiv:cond-mat/0007482.
[6] P. G. Savvidis, B. Kolasa, G. Lee, and S. J. Allen, Resonant Crossover of Terahertz Loss to the Gain of a Bloch oscillating InAs/AlSb Superlattice, Phys. Rev. Lett. **92**, 196802 (2004).
[7] A. Sibille, J. F. Palmier, H. Wang, and F. Mollot, Observation of Esaki-Tsu Negative Differential Velocity in GaAs/AlAs Superlattices, Phys. Rev. Lett. **64**, 52 (1990).
[8] J. Feldmann, K. Leo, J. Shah, D. A. B. Miller, J. E. Cunningham, T. Meier, G. von Plessen, A. Schulze, P. Thomas, and S. Schmitt-Rink, Optical investigation of Bloch oscillations in a semiconductor superlattice, Phys. Rev. B **46**, 7252 (1992).
[9] C. Waschke, H. G. Roskos, R. Schwedler, K. Leo, H. Kurz, and K. Kohler, Coherent Submillimeter-Wave Emission from Bloch Oscillations in a Semiconductor Superlattice, Phys. Rev. Lett. **70**, 3319 (1993).
[10] T. Hyart, K. N. Alekseev, and E. V. Thuneberg, Bloch gain in dc-ac-driven semiconductor superlattices in the absence of electric domains, Phys. Rev. B **77**, 165330 (2008).
[11] T. Hyart, N. V. Alexeeva, J. Mattas, and K. N. Alekseev, Terahertz Bloch Oscillator with a Modulated Bias, Phys. Rev. Lett. **102**, 140405 (2009).
[12] T. Hyart, J. Mattas, and K. N. Alekseev, Model of the Influence of an External Magnetic Field on the Gain of Terahertz Radiation from Semiconductor Superlattices, Phys. Rev. Lett. **103**, 117401 (2009).
[13] M. Ben Dahan, E. Peik, J. Reichel, Y. Castin, and C. Salomon, Bloch Oscillations of Atoms in an Optical Potential, Phys. Rev. Lett. **76**, 4508 (1996).
[14] B. P. Anderson and M. A. Kasevich, Macroscopic quantum interference from atomic tunnel arrays, Science **282**, 1686 (1998).
[15] O. Morsch, J. H. Muller, M. Cristiani, D. Ciampini, and E. Arimondo, Bloch Oscillations and Mean-Field Effects of Bose-Einstein Condensates in 1D Optical Lattices, Phys. Rev. Lett. **87**, 140402 (2001).
[16] M. Cristiani, O. Morsch, J. H. Muller, D. Ciampini, and E. Arimondo, Experimental properties of Bose-Einstein condensates in one-dimensional optical lattices: Bloch oscillations, Landau-Zener tunneling, and mean-field effects, Phys. Rev. A **65**, 063612 (2002).
[17] H. Ott, E. de Mirandes, F. Ferlaino, G. Roati, G. Modugno, and M. Inguscio, Collisionally Induced Transport in Periodic Potentials, Phys. Rev. Lett. **92**, 160601 (2004).

[18] M. Gluck, F. Keck, A. R. Kolovsky, and H. J. Korsch, Wannier-Stark resonances in optical and semiconductor superlattices, Phys. Rep. **366**, 103 (2002).
[19] A. R. Kolovsky and E. N. Bulgakov, Wannier-Stark states and Bloch oscillations in the honeycomb lattice, Phys. Rev. A **87**, 033602 (2013).
[20] R. Bistritzer and A. H. MacDonald, Moiré bands in twisted double-layer graphene, Proc. Natl. Acad. Sci. U.S.A. **108**, 12233 (2011).
[21] Y. Cao, V. Fatemi, A. Demir, S. Fang, S. L. Tomarken, J. Y. Luo, J. D. Sanchez-Yamagishi, K. Watanabe, T. Taniguchi, E. Kaxiras, R. C. Ashoori, and P. Jarillo-Herrero, Correlated insulator behaviour at half-filling in magic-angle graphene superlattices, Nature (London) **556**, 80 (2018).
[22] Y. Cao, V. Fatemi, S. Fang, K. Watanabe, T. Taniguchi, E. Kaxiras, and P. Jarillo-Herrero, Unconventional superconductivity in magic-angle graphene superlattices, Nature (London) **556**, 43 (2018).
[23] Y. Cao, J. Y. Luo, V. Fatemi, S. Fang, J. D. Sanchez-Yamagishi, K. Watanabe, T. Taniguchi, E. Kaxiras, and P. Jarillo-Herrero, Superlattice-Induced Insulating States and Valley-Protected Orbits in Twisted Bilayer Graphene, Phys. Rev. Lett. **117**, 116804 (2016).
[24] Y. Kim, P. Herlinger, P. Moon, M. Koshino, T. Taniguchi, K. Watanabe, and J. H. Smet, Charge inversion and topological phase transition at a twist angle induced van Hove singularity of bilayer graphene, Nano Lett. **16**, 5053 (2016).
[25] A. I. Berdyugin, B. Tsim, P. Kumaravadivel, S. G. Xu, A. Ceferino, A. Knothe, R. Krishna Kumar, T. Taniguchi, K. Watanabe, A. K. Geim, I. V. Grigorieva, and V. I. Falko, Minibands in twisted bilayer graphene probed by magnetic focusing, Sci. Adv. **6**, eaay7838 (2020).
[26] R. Bistritzer and A. H. MacDonald, Electronic Cooling in Graphene, Phys. Rev. Lett. **102**, 206410 (2009).
[27] W. K. Tse and S. Das Sarma, Energy relaxation of hot Dirac fermions in graphene, Phys. Rev. B **79**, 235406 (2009).
[28] J. C. W. Song, M. Y. Reizer, and L. S. Levitov, Disorder-Assisted Electron-Phonon Scattering and Cooling Pathways in Graphene, Phys. Rev. Lett. **109**, 106602 (2012).
[29] See Supplemental Material at http://link.aps.org/supplemental/10.1103/PhysRevLett.126.256803 for detailed estimates of phonon emission and carrier dephasing rates, and a step-by-step derivation of the backaction on the oscillator due to Bloch-oscillating carriers.
[30] L. Ju, B. Geng, J. Horng, C. Girit, M. Martin, Z. Hao, H. A. Bechtel, X. Liang, A. Zettl, Y. R. Shen, and F. Wang, Graphene plasmonics for tunable terahertz metamaterials, Nat. Nanotechnol. **6**, 630 (2011).
[31] H. Yan, X. Li, B. Chandra, G. Tulevski, Y. Wu, M. Freitag, W. Zhu, P. Avouris, and F. Xia, Tunable infrared plasmonic devices using graphene/insulator stacks, Nat. Nanotechnol. **7**, 330 (2012).
[32] H. Yan, Z. Li, X. Li, W. Zhu, P. Avouris, and F. Xia, Infrared spectroscopy of tunable dirac terahertz magneto-plasmons in graphene, Nano Lett. **12**, 3766 (2012).
[33] N. H. Tu, K. Yoshioka, S. Sasaki, M. Takamura, K. Muraki, and N. Kumada, Active spatial control of terahertz plasmons in graphene, Commun. Mater. **1**, 7 (2020).
[34] L. Ateshian, H. Choi, M. Heuck, and D. Englund, Terahertz light sources by electronic-oscillator-driven second harmonic generation in extreme-confinement cavities, arXiv:2009.13029.
[35] I. A. Dmitriev and R. A. Suris, Damping of Bloch oscillations in quantum dot superlattices: A general approach, Semiconductors **36**, 1364 (2002).
[36] A. Rauh and G. H. Wannier, Theory of stark ladders in the optical absorption of solids, Solid State Commun. **15**, 1239 (1974).
[37] I. A. Dmitriev and R. A. Suris, Electron localization and bloch oscillations in quantum-dot superlattices under a constant electric field, Semiconductors **35**, 212 (2001).